Thermal Performance of a Spirally Coiled Finned Tube Heat Exchanger Under Wet-Surface Conditions

Somchai Wongwises*, Paisarn Naphon

Fluid Mechanics, Thermal Engineering and Multiphase Flow Research Lab. (FUTURE), Department of Mechanical Engineering, King Mongkut's University of Technology Thonburi, Bangmod, Bangkok 10140, Thailand

This paper is a continuation of the authors' previous work on spiral coil heat exchangers. In the present study, the heat transfer characteristics and the performance of a spirally coiled finned tube heat exchanger under wet-surface conditions are theoretically and experimentally investigated. The test section is a spiral-coil heat exchanger which consists of a steel shell and a spirally coiled tube unit. The spiral-coil unit consists of six layers of concentric spirally coiled finned tubes. Each tube is fabricated by bending a 9.6 mm diameter straight copper tube into a spiral-coil of four turns. The innermost and outermost diameters of each spiral-coil are 145.0 and 350.4 mm, respectively. Aluminium crimped spiral fins with thickness of 0.6 mm and outer diameter of 28.4 mm are placed around the tube. The edge of fin at the inner diameter is corrugated. Air and water are used as working fluids in shell side and tube side, respectively. The experiments are done under dehumidifying conditions. A mathematical model based on the conservation of mass and energy is developed to simulate the flow and heat transfer characteristics of working fluids flowing through the heat exchanger. The results obtained from the present model show reasonable agreement with the experimental data.

Nomenclature

A : Area
C_p : Specific heat, kJ/(kg ℃)
D : Tube diameter, m
De : Dean number
E_h : Enthalpy effectiveness
E_w : Umidity effectiveness
G : Mass flux, kg/(m² s)
h : Heat transfer coefficient, W/(m² ℃)
h_r : Combined conductance through tube surface and water inside tube, W/(m² ℃)
h_D : Mass transfer coefficient, kg/(m² s)
i : Enthalpy, kJ/kg
i_{fg} : Enthalpy of condensation, kJ/kg
J : Colburn j factor
j : Number of segments
k : Thermal conductivity, W/(m ℃)
Le : Lewis number
M : Mass flow rate per coil, kg/s
m : Total mass flow rate, kg/s
n : Number of coil turns
Nu : Nusselt number
Pr : Prandtl number
Q : Heat transfer rate, W
r : Tube radius, m
R_{min} : Minimum coil radius, m
Re : Reynolds number
R_n : Average radius of curvature, m
T : Temperature, ℃
U : Overall heat transfer coefficient, W/(m² ℃)
δ : Thickness, m
α : Rate of radius change per radian, m/radian
ω : Humidity ratio

* Corresponding Author,
E-mail : somchai.won@kmutt.ac.th
TEL : +662-470-9115; **FAX** : +662-470-9111
Department of Mechanical Engineering, King Mongkut's University of Technology Thonburi, Bangmod, Bangkok 10140, Thailand. (Manuscript **Received** September 1, 2005; **Revised** December 20, 2005)

Subscripts

a : Air
ave : Average
f : Fin
i : Inside
in : Inlet
L : Latent
m : moist air
max : Maximum
min : Minimum
o : Outside
out : Outlet
s : Surface, wall
S : Sensible
sat : Saturated
t : Tube
tot : Total
w : Water
wv : Water vapor

1. Introduction

Due to the high heat transfer coefficient and smaller space requirement compared with straight tubes, curved tubes are the most widely used tubes in several heat transfer applications. Helical and spiral coils are well known types of curved-tubes which have been used in a wide variety of industries. The design and analysis of curved-tube have been studied both analytically and experimentally. Dravid et al.(1971) numerically investigated the effect of secondary flow on laminar flow heat transfer in helically coiled tubes. Patankar et al.(1974) discussed the effect of the Dean number on the temperature fields of three-dimensional parabolic flows for the developing and fully developed regions in helically coiled pipes. Kalb and Seader (1974) studied the fully developed force-convection heat transfer for viscous flow of a constant-properties Newtonian fluid in curved circular tubes with uniform wall-temperature. Yang and Ebadian (1996) solved the k-ε model to analyze the fully developed turbulent convective heat transfer in a circular cross-section helicoidal pipe with finite pitch. Later, Lin and Ebadian (1997) applied the standard k-ε model to investigate three-dimensional turbulent developing convective heat transfer in helical pipes with finite pitches. The effects of pitch, curvature ratio and Reynolds number on the developments of effective thermal conductivity and temperature fields, and local and average Nusselt numbers were discussed. Acharya et al. (2001) numerically studied the phenomenon of steady heat transfer enhancement in coiled-tube heat exchangers due to chaotic particle paths in steady, laminar flow with two different mixings. Xin et al.(1997) experimentally investigated the single-phase and two-phase flow pressure drop in annular helicoidal pipes. Ju et al.(2001) investigated the performance of small bending radius helical-coil pipe. The formulas for the Reynolds number of single-phase flow structure transition, and single-phase and two-phase flow friction factor were obtained. Ali (2001) proposed the pressure drop correlations for fluid flows through regular helical coil tubes. Generalized pressure drop correlations were developed in terms of the Euler number, Reynolds number, and the geometrical group. Chen and Zhang (2003) studied the combined effects of rotation, curvature, and heating/cooling on the flow pattern, friction factor, temperature distribution, and Nusselt number.

Compared to the helically coiled tubes, there are only some researches available on the heat transfer and flow characteristics in the spirally coiled tube. The most productive studies have been continuously carried out by Ho et al.(1995; 1996; 1999). The correlations of the tube-side and air-side heat transfer coefficients reported in literature were used in their simulation to determine the thermal performance of the heat exchanger under cooling and dehumidifying conditions. Experiments were performed to verify the simulation results. Later, Naphon and Wongwises (2003a) modified the mathematical model of Ho et al.(1999) by including the fin efficiency and using other existing heat transfer coefficient correlations to determine the performance and heat transfer characteristics of spiral-coil tube heat exchanger under wet-surface conditions. Due to the lack of the relevant correlations of the

heat transfer coefficients, Naphon and Wongwises (2002) provided the experiments to obtain the air-side and tube-side heat transfer coefficient under wet surface conditions for the spiral coil heat exchanger. The correlation were employed in their mathematical model (Naphon and Wongwises, 2005a). The results obtained from the model are in reasonable agreement with the measured data. The parametric study was done to study the effects of various inlet conditions of working fluids flowing through the spiral coil heat exchanger.

Experiments under dry surface conditions were conducted with the experimental apparatus described in Naphon and Wongwises (2002). The developed correlations were a part of their mathematical model for dry surface conditions (Naphon and Wongwises, 2003b). Later, Naphon and Wongwises (2005b) modified the heat exchanger by including aluminium crimped spiral fins around the coiled tube. Experiments were carried out to determine the correlations of air-side and tube-side heat transfer coefficients under dry and wet surface conditions. These correlations will be used in the present study.

It can be clearly seen that the study on the heat transfer characteristics of the spirally coiled finned tube heat exchanger under wet-surface conditions is still limited. In the present study, main concern is to experimentally and theoretically study the heat transfer characteristics and performance of a spirally coiled finned tube heat exchanger under wet-surface conditions. Experiments are conducted to verify the model results.

2. Experimental Apparatus and Method

Figure 1 shows a schematic diagram of the experimental apparatus. The main components of the system consist of a test section, refrigerant loop, chilled water loop, hot air loop and data acquisition system. Water and air are used as working fluids. The test section is a spirally coiled finned tube heat exchanger. The heat exchanger consists of a shell and spirally coiled finned tube

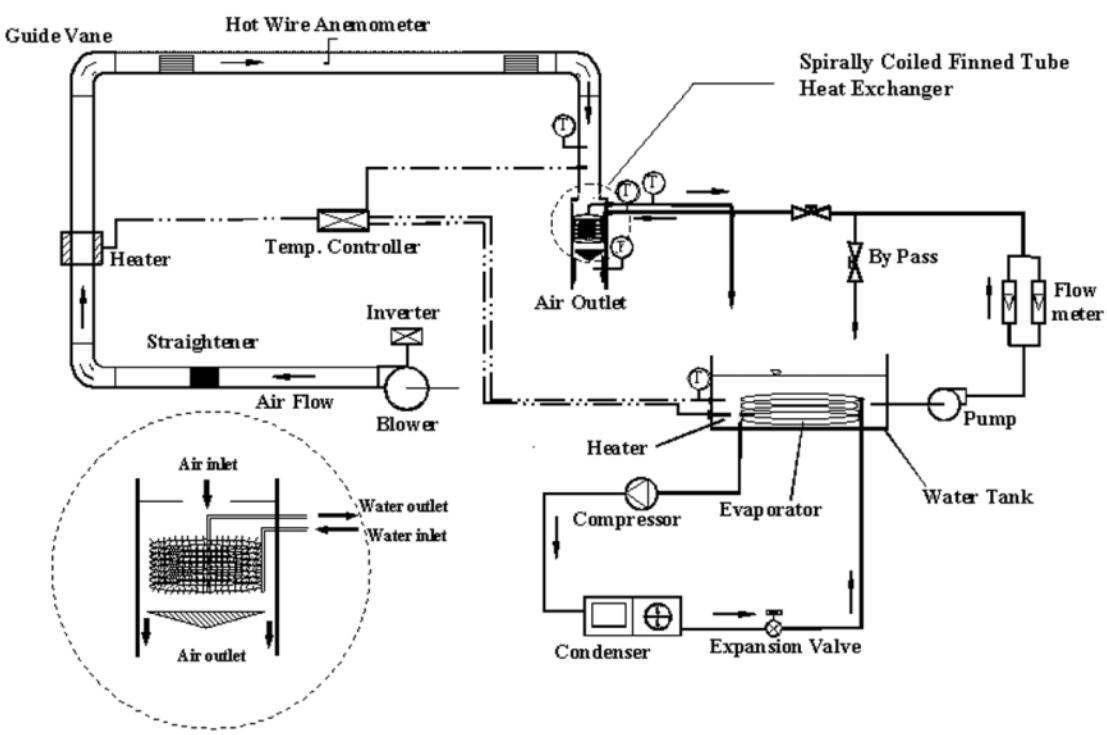

Fig. 1 Schematic diagram of experimental apparatus

unit. The test section and the connections of the piping system are designed such that parts can be changed or repaired easily. In addition to the loop component, a full set of instruments for measuring and control of temperature and flow rate of all fluids is installed at all important points in the circuit.

An open-type wind tunnel is used to conduct the air flow through the heat exchanger. The tunnel is fabricated from zinc, with an inner diameter of 300 mm and a length of 12 m. The duct wall is insulated with a 6.4 mm thick Aeroflex standard sheet. The entering and exiting air temperature of the heat exchanger are measured by type T copper constantan thermocouples extending inside the air channel in which the air flows. The 1 mm diameter thermocouple probes are located at different four positions at the same cross section, 60 cm upstream of the heat exchanger inlet and also four positions at 50 cm downstream of the exit of the heat exchanger. Humidity transmitters are employed to measure the inlet- and outlet-air relative humidities.

The closed-loop of chilled water consists of a 0.3 m^3 storage tank, an electric heater controlled by adjusting the voltage, a stirrer, and a cooling coil immerged inside a storage tank. R22 is used as the refrigerant for chilling the water. Air is discharged by a centrifugal blower into the channel and is passed through a straightener, heater, guide vane, test section, and then discharged to the atmosphere. The purpose of straightener is to avoid the distortion of the air velocity profile. The speed of the centrifugal blower is controlled by the inverter. Air velocity is measured by a hot wire anemometer. The inlet-air temperature is raised to the desired level by using electric heaters controlled by temperature controller. After the temperature of the water is adjusted to achieve the desired level, the chilled water is pumped out of the storage tank, and is passed through a filter, flow meter, test section, and returned to the storage tank. The bypass is used for passing the excess water back to the water tank for the experiments of low water flow rate. The flow rate of the water is measured by a flow meter with a range of 0-10 GPM.

The heat exchanger consists of a steel shell with a spirally coiled finned tube unit. The spiral-coil unit consists of six layers of spirally coiled finned copper tubes. Each tube is constructed by bending a 9.6 mm diameter straight copper tube into a spiral-coil of four turns (Figure 2). The innermost and outermost diameters of each spiral-coil are 145.0 and 350.4 mm, respectively. Aluminium crimped spiral fins with thickness of 0.6 mm and outer diameter of 28.4 mm are placed around the tube. The edge of fin at the inner diameter is corrugated. Schematic diagram of fin is shown in Fig. 3. Each end of the spirally coiled finned tube is connected to vertical manifolds with outer diameter of 28.5 mm. The copper constantan thermocouples are installed at the third layer of the spiral-coil unit from the uppermost layer, each with two thermocouples to measure the water temperature and wall temperature. The water temperature is measured in five positions with 1 mm diameter probe extending inside the tube in which the water flows. The thermocouples are also mounted at five positions on the tube wall surface to measure the wall temperature. Thermocouples are soldered into a small hole drilled 0.5 mm deep into tube wall surface and fixed with special glue applied to the outside surface of the copper tubing. With this method, thermocouples are not biased by the fluid temperatures. The dimensions of the heat exchanger are listed in Table 1.

In the experiment, an overall energy balance was performed to estimate the extent of any heat losses or gains from the surrounding. Experiments

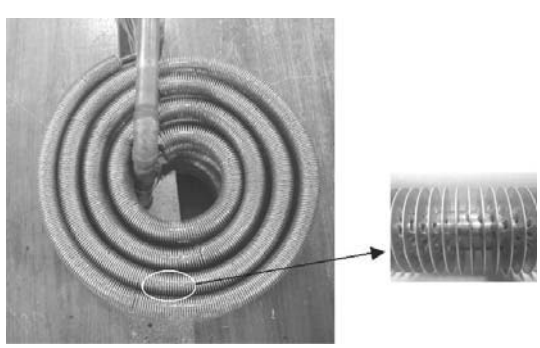

Fig. 2 Photograph of the spirally coiled finned tube unit used in the present study

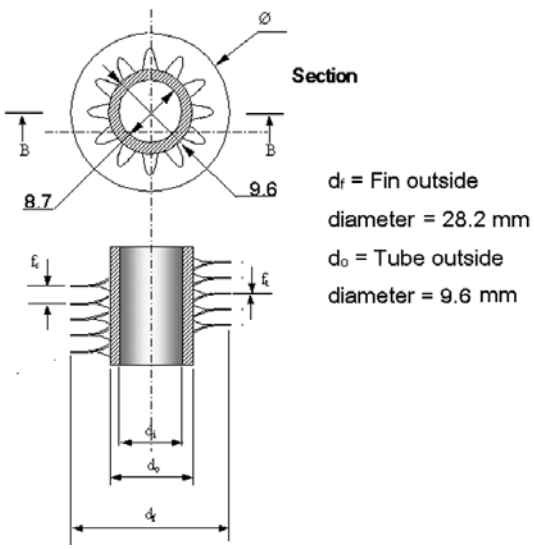

Fig. 3 Schematic diagram of crimped spiral fin

Table 1 Dimensions of the spirally coiled finned tube heat exchanger

Parameters	Dimensions
Outer diameter of tube, mm	9.6
Inner diameter of tube, mm	8.7
Innermost diameter of spiral coil, mm	145.0
Outermost diameter of spiral coil, mm	350.4
Number of coil turns	4
Number of layer of spiral coils	6
Distance between the spiral coil layer, mm	31.4
Diameter of shell, mm	430
Length of shell, mm	350
Diameter of hole at air inlet, mm	125
Diameter of closed plate at air outlet, mm	360
Fin pitch, mm	3.1
Fin height, mm	9.3
Fin thickness, mm	0.35
Number of fins per metre	310

were conducted with various inlet temperatures and flow rates of hot air and chilled water entering the test section. The chilled-water flow rate was increased in small increments while the hot-air flow rate, inlet chilled water and hot-air temperatures were kept constant. The inlet hot air and inlet chilled water temperatures were adjusted to achieve the desired level by using electric heaters controlled by temperature controllers. Before any data were recorded, the system was allowed to approach the steady state. The range of experimental conditions in this study and uncertainty of the measurement are given in Tables 2 and 3, respectively.

Table 2 Experimental conditions

Variables	Range
Inlet-air temperature, ℃	55-60
Inlet-water temperature, ℃	7.5-20
Air mass flow rate, kg/s	0.02-0.20
Water mass flow rate, kg/s	0.04-0.25

Table 3 Uncertainty of measurement

Instruments	Accuracy	Uncertainty
Hot wire anemometer (air velocity, m/s)	2.0%	±0.23
Rotameter (water mass flow rate, kg/s)	0.2%	±0.003
Type T thermocouple	0.1%	±0.03
Data logger, (℃)	0.04%	
Humidity transmitter (%RH)	0.5%	±0.22

3. Mathematical Modelling

For the study of the performance of the spirally coiled finned tube heat exchanger under wet surface conditions, a computer program developed at FUTURE was used. As shown in Fig. 1, the hot air flows into the center core and then flows across the spiral coils, radially outwards to the inner wall of the shell before leaving the heat exchanger at the air outlet section. In the model, the study of the physical behaviour and parameters is developed based on the fundamental principal of thermodynamics. The mathematical model is based on that of Ho et al.(1999), and Naphon and Wongwises (2003a). Fig. 4 shows a schematic diagram of the simulation approach. The model developed is based on the following main assumptions:

(1) Steady flow of air and water

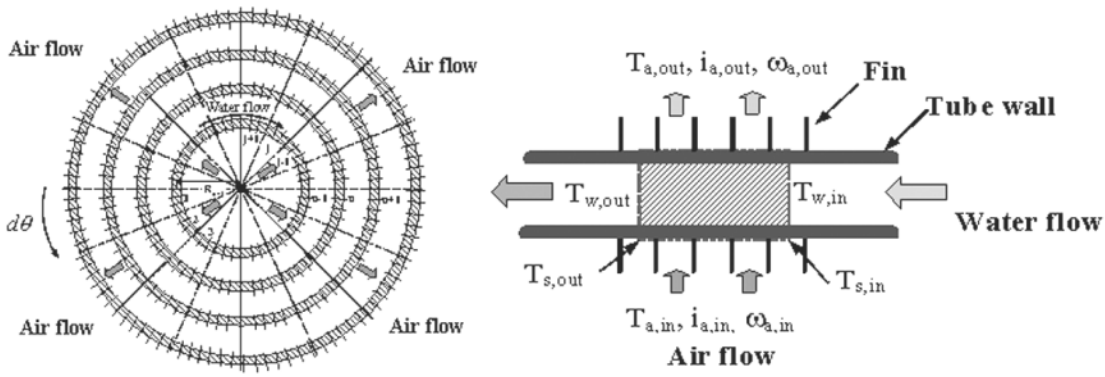

Fig. 4 Schematic diagram of simulation approach and control volume of each segment

(2) Neligible heat transfer to the surrounding

(3) Constant air-side (and water-side) convective heat transfer coefficients at each section of a coil turn in the horizontal plane

(4) Neligible thermal resistance of the liquid film

(5) Constant thermal conductivity of the spirally coiled tube

3.1 Air-side heat transfer

While air passes over a cooling coil having a surface temperature below its dew point temperature, the air is chilled below the dew point, thus condensing out moisture. Considering the control volume of each segment in Fig. 4, the total heat transfer rate is determined from the sum of latent heat and sensible heat as follows:

$$dQ_T = dQ_S + dQ_L \tag{1}$$

where dQ_T, dQ_S, and dQ_L are the total heat, sensible heat and latent heat, respectively.

$$dQ_S = h_o dA_{o,tot}(T_{a,in} - T_s) \tag{2}$$

where h_o is the air-side heat transfer coefficient, $dA_{o,tot}$ is the outside surface area including the area of the fins, $T_{a,in}$ is the inlet-air temperature, and T_s is the tube surface temperature.

As moisture is condensed, the heat released is determined by

$$dQ_L = dM_{wv} i_{fg} \tag{3}$$

where i_{fg} is the enthalpy of condensation and dM_{wv} is the mass transfer rate of the water vapor, defined as

$$dM_{wv} = h_D dA_{o,tot}(\omega_{a,in} - \omega_{sat,s}) \tag{4}$$

where h_D is the mass transfer coefficient, $\omega_{a,in}$ is the inlet humidity ratio of air, and $\omega_{sat,s}$ is the humidity ratio at saturated conditions at the tube surface temperature.

Substituting Eq. (2), Eq. (3) and Eq. (4) into Eq. (1) gives

$$dQ_T = \left(\frac{h_o}{C_{p,m}} dA_{o,tot}\right) \left(C_{p,m}(T_{a,in} - T_s) + \frac{1}{Le}(\omega_{a,in} - \omega_{sat,s}) i_{fg}\right) \tag{5}$$

where the Lewis number, Le, is defined by

$$Le = \frac{h_o}{h_D C_{p,m}}$$

The specific heat of the moist air, $C_{p,m}$, is the sum of the specific heat of dry air and water vapor:

$$C_{p,m} = C_{p,a} + \omega_a C_{p,wv} \tag{6}$$

Substituting Eq. (6) into Eq. (5) and assuming Le is approximately equal to 1, we get

$$dQ_T = \left(\frac{h_o dA_{o,tot}}{C_{p,m}}\right)(i_{a,in} - i_{sat,s}) \tag{7}$$

where $i_{a,in}$ is the inlet enthalpy of air, and $i_{sat,s}$ is the enthalpy at saturated conditions at tube surface temperature.

3.2 Water-side heat transfer

The heat transfer rate in terms of the water flow rate can be given as:

$$dQ_T = M_w C_{p,m} dT_w \tag{8}$$

The heat transfer rate to the water can be expressed as:

$$dQ_T = h_r dA_{o,tot}(T_s - T_w) \tag{9}$$

where

$$\frac{1}{e_r} = \frac{\delta_t dA_{o,tot}}{k_t dA_{ave}} + \frac{dA_{o,tot}}{dA_i h_i} \tag{10}$$

where δ_t is the tube thickness, dA_{ave} is the average surface area, and h_r is the combined conductance through the tube surface and water inside tube.

3.3 Energy balance

Considering the energy balance over the control volume for each segment, we get

$$\frac{h_o dA_{o,tot}}{C_{p,m}}(i_{a,in} - i_{sat,s}) = h_r dA_{o,tot}(T_s - T_w) \tag{11}$$

Rearranging gives

$$\frac{h_o}{h_r C_{p,m}} = \frac{(T_s - T_w)}{(i_{a,in} - i_{sat,s})} = Rc \tag{12}$$

The enthalpy of the saturated air, $i_{sat,s}$, as described by Ho et al.(1996) is used for the present study.

$$i_{sat,s} = 10.90748 + 1.22045\,T_s + 0.05652\,T_s^2 \tag{13}$$

Substituting Eq. (13) into Eq. (12) and rearranging, we get

$$0.05652\,T_s^2 + \left[1.22045 + \frac{1}{Rc}\right]T_s + \left[10.90749 - i_{a,in} - \frac{T_w}{Rc}\right] = 0 \tag{14}$$

The energy balance over the control volume for each segment may be written in terms of the water flow rate as follows:

$$\begin{aligned} &h_r dA_{o,tot}\left(\frac{T_{s,out} + T_{s,in}}{2} - \frac{T_{w,out} - T_{w,in}}{2}\right) \\ &= Mw C_{p,w}(T_{w,out} - T_{w,in}) \\ &= M_w C_{p,w}(T_{w,out} - T_{w,in}) \end{aligned} \tag{15}$$

On rearranging, we get

$$T_{w,out} = \frac{1}{\beta+1}(\beta(T_{s,out} + T_{s,in}) - T_{w,in}(\beta - 1)) \tag{16}$$

where

$$\beta = \frac{h_r dA_{o,tot}}{2 M_w C_{p,w}} \tag{17}$$

Eq. (14) can be written using $T_{s,out}$ and $T_{s,in}$, so

$$0.05652\,T_{s,out}^2 + \left[1.22045 + \frac{1}{Rc}\right]T_{s,out} + \left[10.90749 - i_{a,in} - \frac{T_{w,out}}{Rc}\right] = 0 \tag{18}$$

and

$$0.05652\,T_{s,in}^2 + \left[1.22045 + \frac{1}{Rc}\right]T_{s,in} + \left[10.90749 - i_{a,in} - \frac{T_{w,in}}{Rc}\right] = 0 \tag{19}$$

Substituting Eq. (16) into Eq. (18) then gives

$$0.05652\,T_{s,out}^2 + \left[1.22045 + \frac{1}{Rc} - \frac{\beta}{Rc(\beta+1)}\right]T_{s,out} + 10.90749 - i_{a,in} - \frac{1}{Rc(\beta+1)}[\beta T_{s,in} - (\beta - 1)\,T_{w,in}] = 0 \tag{20}$$

3.4 Fin efficiency

The overall surface effectiveness, η_o which is defined as the ratio of the effective heat transfer area to the total heat transfer area, can be expressed in terms of fin efficiency, η, fin surface area, A_f, and total surface area, $A_{o,tot}$, as follows:

$$\eta_o = \eta_o = 1 - \frac{A_f}{A_{o,tot}}(1 - \eta) \tag{21}$$

The fin efficiency, η, is determined by the method proposed by Schmidt (1949) as follows:

$$\eta = \frac{\tanh(\varphi r_o \phi)}{\varphi r_o \phi} \tag{22}$$

where

$$\phi = \left(\frac{R_f}{r_o} - 1\right)\left[1 + 0.35 \ln\left(\frac{R_f}{r_o}\right)\right] \tag{23}$$

For wet-surface conditions, the wet fin efficiency can be determined by equation developed by McQuiston (1994) as follows:

$$\varphi^2 = \frac{2h_o}{k_f \delta_f}\left(1 + \frac{B_{sa} \cdot i_{fg}}{C_{p,a}}\right) \tag{24}$$

$$B_{sa} = \frac{\omega_{sat,s} - \omega_{a,ave}}{T_{sat,s} - T_{a,ave}} \tag{25}$$

The specific humidity of air at saturated conditions is a function of the tube wall temperature. It can be obtained from the correlation given by Liang (1999).

$$\omega_{sat,s}=(3.7444+0.3078\,T_s+0.0046\,T_s^2+0.0004\,T_s^3)\cdot 10^{-3} \quad (26)$$

where R_f is the fin radius, r_o is the outer tube radius, k_f is the thermal conductivity of the fin, δ_f is the fin thickness, $T_{a,ava}$ is the average temperature of air, $\omega_{a,ave}$ is the average specific humidity of air, and $T_{sat,ave}$ is the saturated temperature of the water film which is equal to the average wall temperature, $T_{s,ave}$.

4. Solution Methodology

A schematic diagram shown in Fig. 4 is used to simulate each layer of spiral coil tube. Each coiled tube is divided into four circular coil turns having the following mean radius:

$$R_n=(R_{\min}+(2n-1)\,a\pi) \quad (27)$$

where $R_{\min}$ is the minimum coil radius, n is the number of coil turns, and a is the radius change per radian.

As shown in Fig. 4, each circular coil turn is divided into several segments. The calculation is done segment by segment along the circular coil turn by beginning at a segment of the innermost coil turn. The correlations proposed by Naphon and Wongwises (2005b) are used to calculate the tube-side and air-side heat transfer coefficients under wet surface conditions of the spirally coiled finned tube.

Tube-side heat transfer coefficient:

$$Nu_i\frac{h_i d_i}{k}=10.0De^{0.464}Pr^{-0.755} \quad (28)$$

for $300<De<2200$, $Pr\geq 5$

Air-side heat transfer coefficient:

$$J=\frac{h_o}{G_{\max}C_{p,m}}Pr^{2/3}=0.029Re_o^{-0.202} \quad (29)$$

for $Re_o<6{,}000$

In addition, the heat exchanger dimensions and properties of working fluids, as well as the operating conditions, are also needed. The iteration process is described as follows:

(1) The outlet-water temperature and fin efficiency are assumed.

(2) The fin efficiency is assumed.

(3) Eqs. (16), (19) and (20) are solved simultaneously by using the Newton-Raphson method to determine the tube surface temperature at inlet ($T_{s,in}$), tube surface temperature at outlet ($T_{s,out}$), the inlet water temperature ($T_{w,in}$) and outlet water temperatures, ($T_{w,out}$) at segment 1.

(4) The fin efficiency and overall surface effectiveness are determined.

(5) The calculated fin efficiency is compared with the assumed one. If the difference is within 10^{-6}, the calculations are ended, and if not, new fin efficiency value of the first segment is tried again, the computations are repeated until convergence is obtained.

(6) The computation described above is next performed at segment 2, 3, 4, ⋯ and the remaining segments until the last segment.

(7) The same computation is performed for the next circular coil, the computation is terminated when the calculation at the last segment of the outermost coil turn is finished.

(8) The calculated water temperature at the last segment of the outermost coil turn is compared with the inlet-water temperature (an initial condition). If the difference is within 10^{-6}, the calculations are ended, and if not, new outlet-water temperature for the first segment at the innermost coil turn is tried again, the computations are repeated until convergence is obtained.

5. Results and Discussion

Figures 5 and 6 show the variation of the water and tube wall temperatures with the position along the spiral tube for different air mass flow rates. The water and tube wall temperatures are measured at the 3rd layer from the uppermost layer. The 1st and 5th positions are represented as the innermost and the outermost turns of the spiral coil, respectively. The chilled water entering the outermost turn flows along the spiral tube and flows out at the innermost turn. The hot air enters the heat exchanger at the center of the shell and flows radially across the spiral tubes to the periphery before leaving the heat exchanger at the air outlet section. The experiments are carried out under dehumidifying conditions, for an air mass flow rate of 0.25 kg/s, inlet-water and-air temperatures of 12.5 and 50℃, respectively. The

heat transfer processes under wet-surface conditions are more complex than those under dry-surface conditions. In general, the presence of condensate film on the coil surface has significant ability to enhance the heat transfer at the condensate-air interface. This phenomenon can be clearly explained as follows: firstly, due to a generated locally turbulent air flow resulted from the water film and water drop on the tube surface. Secondly, due to the increase of heat transfer area. However, due to the increase of the water film thickness, thermal resistance increases. This results in a reduction of heat transfer rate. But, this effect is very small as compared to the first two effects. As expected, the water and tube wall temperatures increase along the tube. It should be noted that when the water mass flow rate, the inlet-water and-air temperatures are kept constant at the same position, the water and tube wall temperatures at lower water mass flow rates are lower than at higher ones. Figures 5 and 6 also compare the results obtained from the experiment and those obtained from the model. It can be clearly seen from figures that the results obtained from the model slightly overpredict the measured data.

Figures 7 and 8 show the variation of the outlet-air temperature with air mass flow rate at

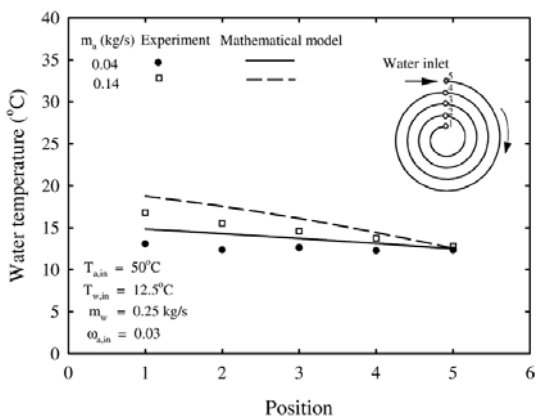

Fig. 5 Variation of water temperature with position along the spiral coil for difference air mass flow rates

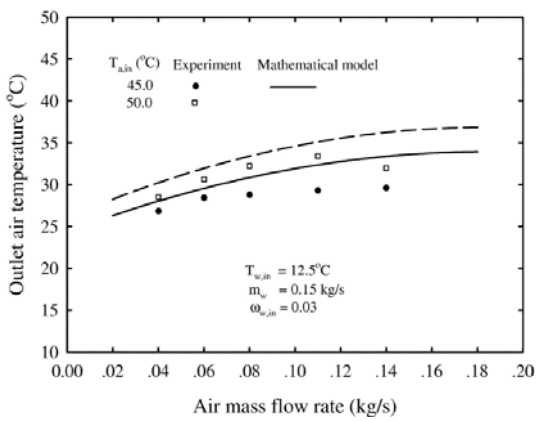

Fig. 7 Variation of the outlet-air temperature with air mass flow rate for different inlet-water temperatures at $T_{w,in}$=12.5℃, m_w=0.15 kg/s

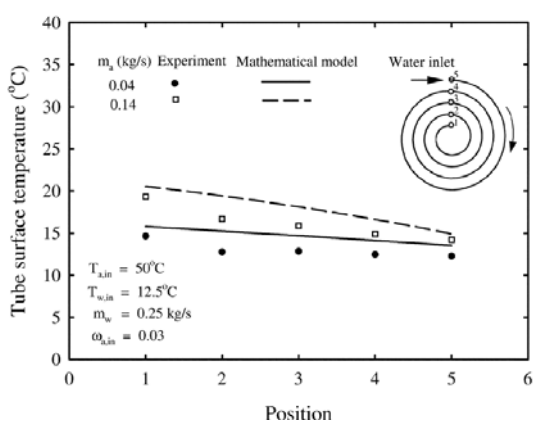

Fig. 6 Variation of tube surface temperature with position along the spiral coil for difference air mass flow rates

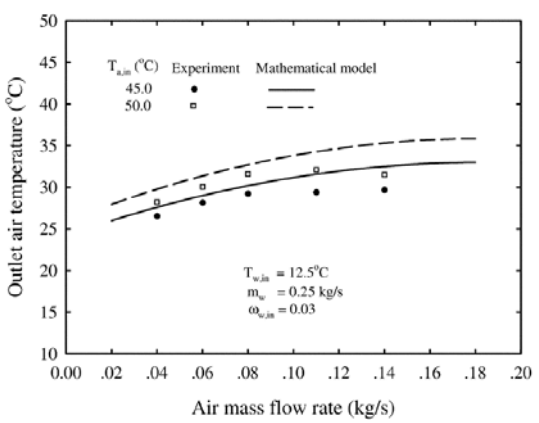

Fig. 8 Variation of the outlet-air temperature with air mass flow rate for different inlet-water temperatures at $T_{w,in}$=12.5℃, m_w=0.25 kg/s

$T_{w,in}$=12.5℃, $\omega_{a,in}$=0.03 for the different inlet-air temperatures of 45 and 50℃. For a given water mass flow rate and inlet-air temperature, the outlet-air temperature tends to increase with increasing air mass flow rate. In addition, at the same air mass flow rate, the outlet-air temperature at 45℃ is lower than at 50℃ across the range of air mass flow rates. As shown in the figure, verification of the present numerical simulation is done by comparison with experimental data. As shown in Figs. 5-6, the results obtained from the model slightly overpredict the present measured data. Figs. 9 and 10 show the variation of the outlet-air temperature with air mass flow rate for the different water mass flow rates of 0.15, 0.20 and 0.25 kg/s. In general, the same explanation described above as for Figs. 7-8 can be given. However, the effect of the water mass flow rate on the outlet-air temperature in the present experiment is quite low.

Figures 11 and 12 show the variation of the outlet-water temperature with air mass flow rate for the different inlet-air temperatures of 45 and 50℃. At a specific inlet-air temperature, inlet-water temperature and water mass flow rate, the increase of the outlet-water temperature caused by the increase of the heat transfer rate results in an increase of the outlet-air temperature. As the

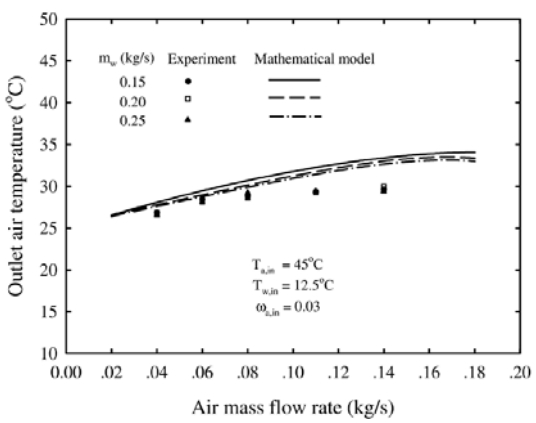

Fig. 9 Variation of the outlet-air temperature with air mass flow rate for different water mass flow rates at $T_{a,in}$=45℃, $T_{w,in}$=12.5℃

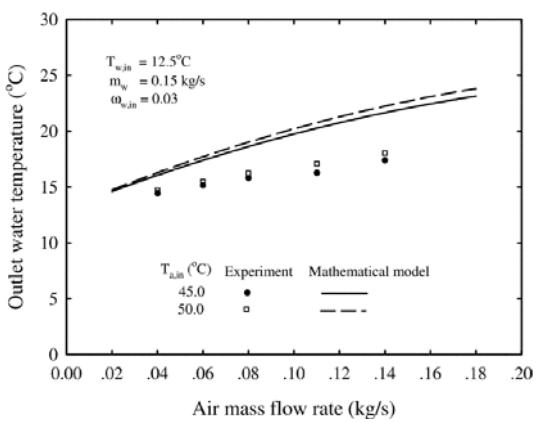

Fig. 11 Variation of the outlet-water temperature with air mass flow rate for different inlet-air temperatures at $T_{w,in}$=12.5℃, m_w=0.15 kg/s

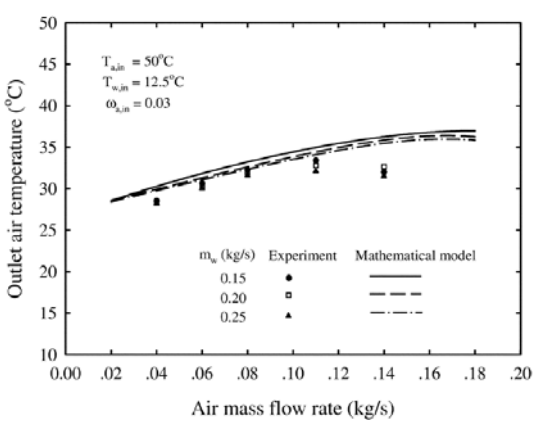

Fig. 10 Variation of the outlet-air temperature with air mass flow rate for different water mass flow rates at $T_{a,in}$=50℃, $T_{w,in}$=12.5℃

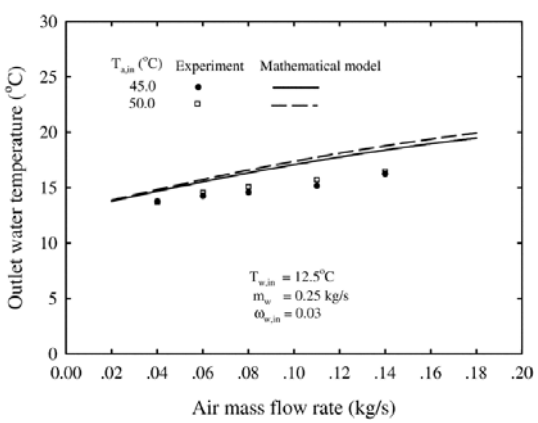

Fig. 12 Variation of the outlet-water temperature with air mass flow rate for different inlet-air temperatures at $T_{w,in}$=12.5℃, m_w=0.25 kg/s

outlet-air temperature increases, the temperature difference between inlet and outlet-air temperature decreases. Therefore, one way of keeping the heat transfer rate equal to the water side is by increasing the air mass flow rate. Therefore, it can be clearly seen that the outlet-water temperature increases with increasing air mass flow rate. At the same air mass flow rate, the outlet-water temperature at $T_{a,in}$=50℃ tends to be higher than at $T_{a,in}$ 45℃. The reason for this is similar to the one as described above. At a specific inlet-water temperature, water mass flow rate and air mass flow rate, as the outlet-water temperature increases, the outlet-air temperature and heat transfer rate increase. Therefore, in order to keep the heat transfer rate equal to the water-side heat transfer rate, the inlet-air temperature must be increased. Considering the results obtained from the present model and those obtained from the experiment, it can be clearly seen from figure that the predicted outlet-water temperature is higher than the measured one. This may be due to the fact that the thermal resistance of the liquid film that covers the tube surface is not included in the mathematical model causing higher heat transfer rate from hot air to chilled water.

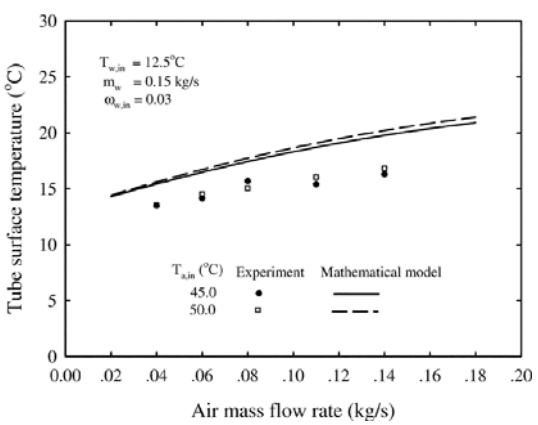

Fig. 13 Variation of the tube surface temperature with air mass flow rate for different inlet-air temperatures at $T_{w,in}$=12.5℃, m_w=0.15 kg/s

Figures 13 and 14 show the variations of the tube surface temperatures with air mass flow rate. The tube surface temperature is measured at the 3rd layer from the uppermost layer in five positions in which the water flows. It can be seen from both figures that the trends of the tube surface temperature are similar to those of the outlet-water temperature curves as shown in Figures 11 and 12. Again, considering the predicted and measured results, it is found that the model over-predicts the measured data.

Figures 15-18 show the variation of the heat transfer rate with air mass flow rate. As expected, the heat transfer rate is directly proportional to the air mass flow rate. In addition, it can be noted that the inlet-air temperature and water mass flow rate strongly affect the heat transfer rate, however the effect of inlet-air temperature on the heat

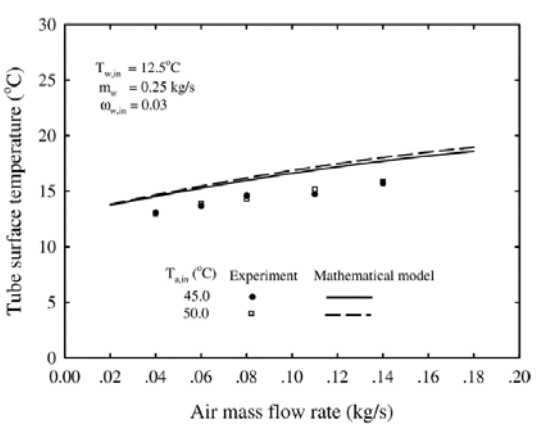

Fig. 14 Variation of the tube surface temperature with air mass flow rate for different inlet-air temperatures at $T_{w,in}$=12.5℃, m_w=0.25 kg/s

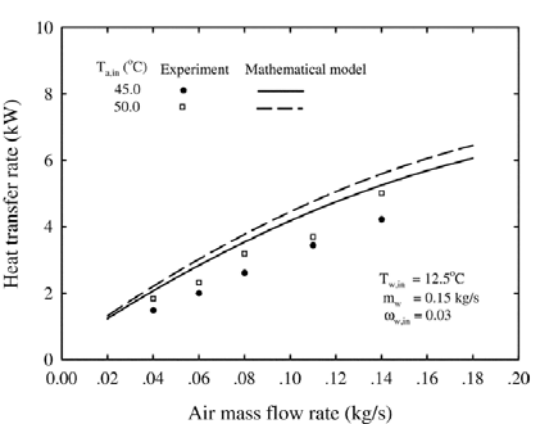

Fig. 15 Variation of the heat transfer rates with air mass flow rate for different inlet-air temperatures at $T_{w,in}$=12.5℃, m_w=0.15 kg/s

transfer rate can be clearly seen at higher air mass flow rate. Figures 15-18 also show the comparison between the predicted results and the measured data. It can be clearly seen from these figures that the results obtained from the experiment are lower than those obtained from the model. This may be due to not including the thermal resistance of the liquid film into the mathematical model as described before. In addition, because the straight copper tube is bent, the cross sectional area of the tube is not circular causing the imperfect attachment between the annular helical fin and the tube surface, especially at the innermost turn. This results in the decreasing of heat transfer rate. However, the corrugated edge of helical fin causing larger heat transfer area and higher turbulence of air flow results in the increasing of the heat transfer rate. The proposed model, therefore, simulates the experimental data fairly well.

Figures 19-20 illustrate the variations of the enthalpy effectiveness and humidity effectiveness with air mass flow rate, respectively at $T_{w,in}$= 12.5℃, m_w=0.15 kg/s, $\omega_{a,in}$=0.03, for different inlet-air temperatures of 45 and 50℃. For the whole range of inlet-water temperature, it is found that the tube surface temperature is always lower than the dew-point temperature of the air.

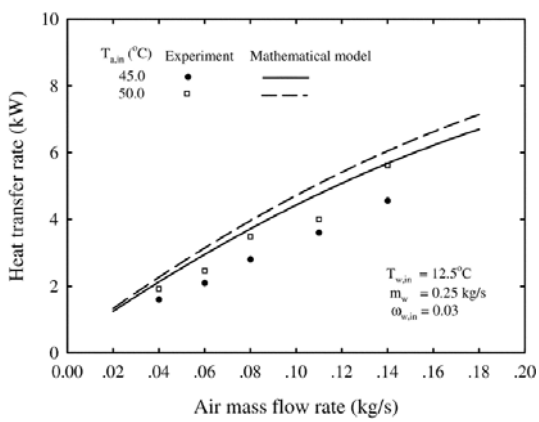

Fig. 16 Variation of the heat transfer rates with air mass flow rate for different inlet-air temperatures at $T_{w,in}$=12.5℃, m_w=0.25 kg/s

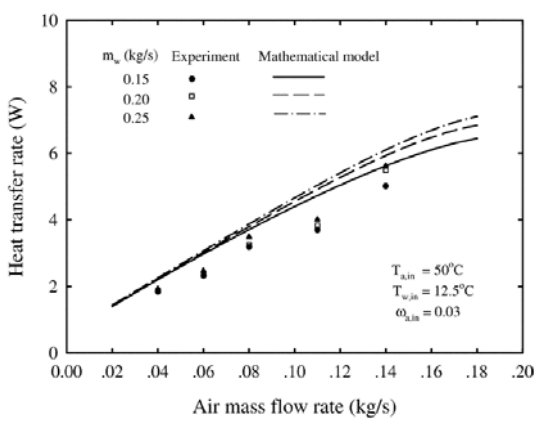

Fig. 18 Variation of the heat transfer rates with air mass flow rate for different water mass flow rates at $T_{a,in}$=50℃, $T_{w,in}$=12.5℃

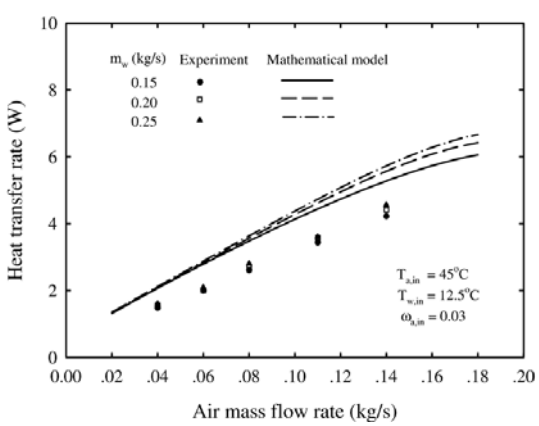

Fig. 17 Variation of the heat transfer rates with air mass flow rate for different water mass flow rates at $T_{a,in}$=45℃, $T_{w,in}$=12.5℃

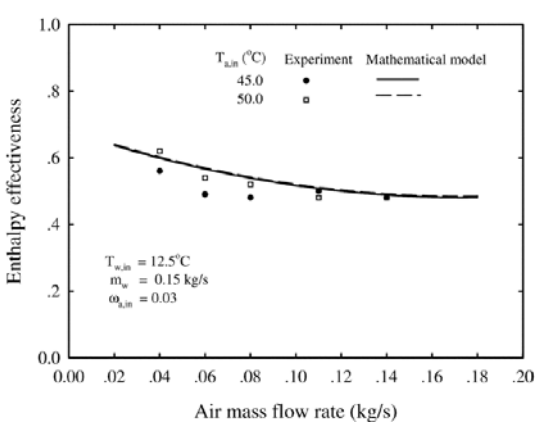

Fig. 19 Variation of the enthalpy effectiveness with air mass flow rate for different inlet-air temperatures at $T_{w,in}$=12.5℃, m_w=0.15 kg/s

This results in condensing out of the moisture. The total load-removal performance and the latent load-removal performance of the spiral-coil heat exchanger can be presented in term of the enthalpy effectiveness and humidity effectiveness, respectively, as follows

Enthalpy effectiveness,

$$E_h=\frac{i_{a,in}-i_{a,out}}{i_{a,in}-i_{sat,s}} \tag{30}$$

Humidity effectiveness,

$$E_w=\frac{\omega_{a,in}-\omega_{a,out}}{\omega_{a,in}-\omega_{sat,s}} \tag{31}$$

It is found from these figures that the enthalpy effectiveness and the humidity effectiveness decrease with increasing air mass flow rate for a given inlet-water temperature, inlet-air humidity ratio, and water mass flow rate. Increasing of the air mass flow rate affects directly the outlet enthalpy, $i_{a,out}$, enthalpy of saturated air, $i_{sat,s}$, outlet humidity ratio, $\omega_{a,out}$, and humidity ratio of saturated air, $\omega_{sat,s}$. However, the increases of the outlet enthalpy and outlet humidity ratio of air are larger than those of the enthalpy of saturated air and humidity ratio of saturated air. Therefore, the enthalpy effectiveness and humidity effectiveness tend to decrease with increasing air mass flow rate. At a given air mass flow rate, higher inlet-air temperature leads to the increase in enthalpy effectiveness and humidity effectiveness. The results show the same trend for m_w= 0.25 kg/s (Figures 21-22). Effect of the water mass flow rate on the enthalpy effectiveness and humidity effectiveness are also shown in Figures 23 and 24. It can be clearly seen from both figures that the enthalpy effectiveness and humidity effectiveness are inversely proportional to the air mass flow rate for a given water mass flow rate. In the present experiment, effect of the water mass flow rate on the enthalpy effectiveness and humidity effectiveness is quite low. The agreement between the simulation and measured data is fairly well.

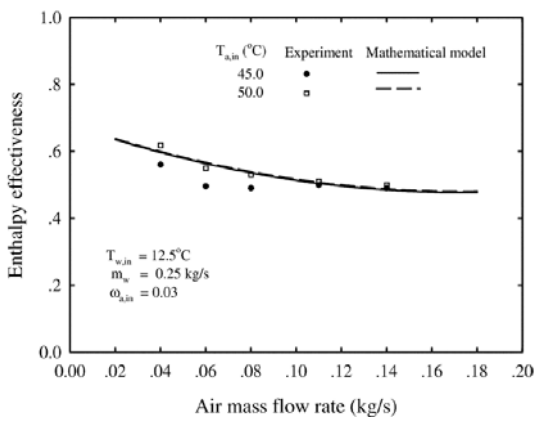

Fig. 21 Variation of the enthalpy effectiveness with air mass flow rate for different inlet-air temperatures at $T_{w,in}$=12.5℃, m_w=0.25 kg/s

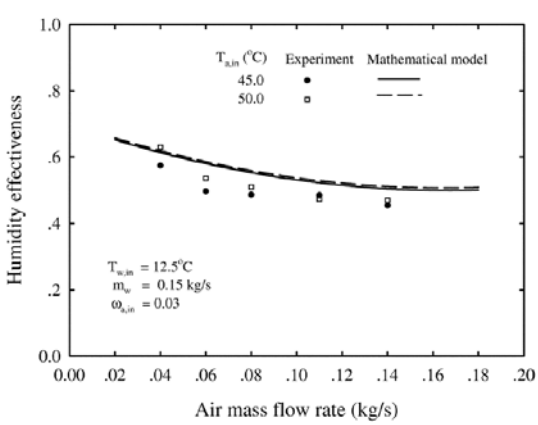

Fig. 20 Variation of the humidity effectiveness with air mass flow rate for different inlet-air temperatures at $T_{w,in}$=12.5℃, m_w=0.15 kg/s

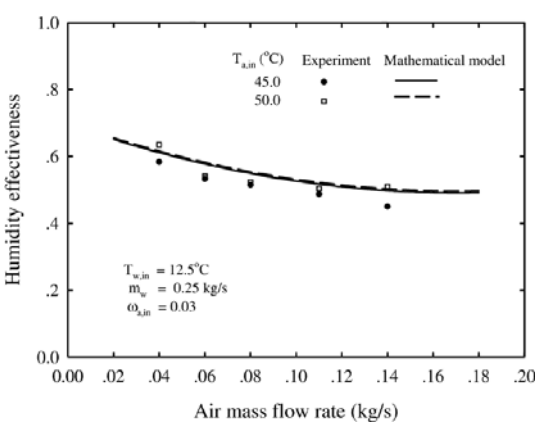

Fig. 22 Variation of the humidity effectiveness with air mass flow rate for different inlet-air temperatures at $T_{w,in}$=12.5℃, m_w=0.25 kg/s

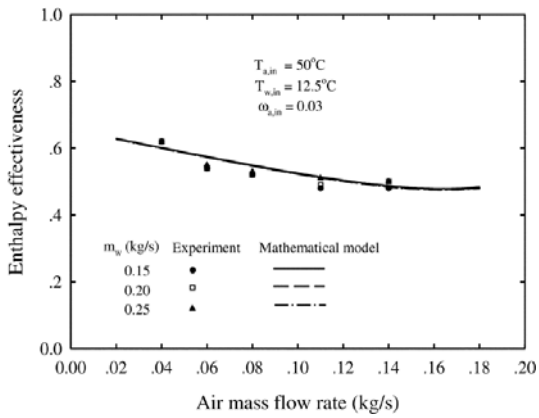

Fig. 23 Variation of the enthalpy effectiveness with air mass flow rate for different water mass flow rates at $T_{a,in}$=50℃, $T_{w,in}$=12.5℃

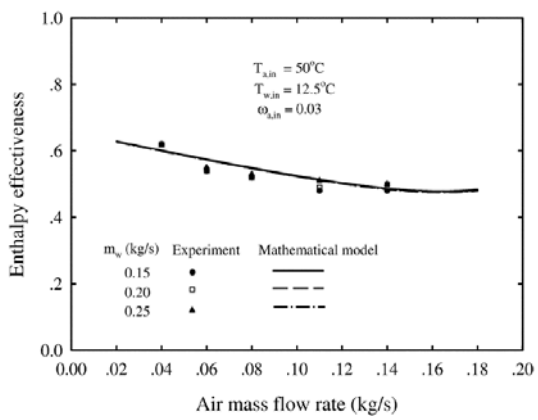

Fig. 24 Variation of the humidity effectiveness with air mass flow rate for different water mass flow rates at $T_{a,in}$=50℃, $T_{w,in}$=12.5℃

6. Conclusions

New experimental data of the heat transfer characteristics and the performance of a spirally coiled finned tube heat exchanger under wet-surface conditions are presented. The results obtained from the developed model are validated by comparing with the measured data. The effects of the inlet conditions of the working fluids flowing through the heat exchanger are discussed. The following conclusions can be given :

(1) There is reasonable agreement between the results obtained from the experiment and those from the developed model.

(2) Air mass flow rate and inlet-air temperature have significant effect on the increase of the outlet-air and-water temperatures.

(3) The outlet-air and-water temperatures decrease with increasing water mass flow rate.

(4) The enthalpy effectiveness and humidity effectiveness decrease as the air mass flow rates increases.

(5) In addition, it is found from the results that the liquid film has significant effect on the heat transfer characteristics and performance of the heat exchanger.

Acknowledgments

The authors would like to express their appreciation to the Thailand Research Fund (TRF) for providing financial support for this study.

References

Acharya, N., Sen, M. and Chang, H. C. 2001, "Analysis of Heat Transfer Enhancement in Coiled-tube Heat Exchangers," *International Journal of Heat and Mass Transfer*, 44, pp. 3189～3199.

Ali, S., 2001, "Pressure Drop Correlations for Flow Through Regular Helical Coil Tubes," *Fluid Dynamics Research*, 28, pp. 295～310.

Chen, H. and Zhang, B., 2003, "Fluid Flow and Mixed Convection Heat Transfer in a Rotating Curved Pipe," *International Journal of Thermal Science*, 42, pp. 1047～1059.

Dravid, A. N., Smith, K. A., Merrill, E. W. and Brian, P. L. T., 1971, "Effect of Secondary Fluid on Laminar Flow Heat Transfer in Helically Coiled Tubes," *AIChE. Journal*, 17, pp. 1114～1122.

Ho, J. C. Wijeysundera, N. E. and Rajasekar, S., 1996, "Study of a Compact Spiral-coil Cooling and Dehumidifying Heat Exchanger Unit," *Applied Thermal Engineering*, 16, pp. 777～790.

Ho, J. C., Wijeysundera, N. E., Rajasekar, S. and Chandratilleke, T. T., 1995, "Performance of a Compact Spiral Coil Heat Exchange," *Heat Recovery System & CHP*, 15, pp. 457～468.

Ho, J. C., Wijeysundera, N. E. and Rajasekar, S., 1999, "An Unmixed-air Flow Model of a

Spiral Cooling Dehumidifying Heat Transfer," *Applied Thermal Engineering*, 19, pp. 865～883.

Ju, H., Huang, Z., Xu, Y., Duan, B. and Yu, Y., 2001, "Hydraulic Performance of Small Bending Radius Helical Coil-pipe," *Journal of Nuclear Science and Technology*, 18, pp. 826～831.

Kalb, C. E. and Seader, J. D., 1974, "Fully Developed Viscous-Flow Heat Transfer in Curved Circular Tubes with Uniform Wall Temperature," *AIChE. Journal*, 20, pp. 340～346.

Liang, S. Y., Liu, M., Wong, T. N. and Nathan, G. K., 1999, "Analytical Study of Evaporator Coil in Humid Environment," *Applied Thermal Engineering*, 19, pp. 1129～1145.

Lin, C. X. and Ebadian, M. A., 1997, "Developing Turbulent Convective Heat Transfer in Helical Pipes," *International Journal of Heat and Mass Transfer*, 40, pp. 3861～3873.

McQuiston, F. C. Parker, J. D., 1994, "Heating, Ventilating, and Air Conditioning," *John Wiley & Sons, Inc.*, 4th Edition.

Naphon, P. and Wongwises, S., 2003a, "Investigation of the Performance of a Spiral-coil Finned Tube Heat Exchanger under Dehumidifying Conditions," *Journal of Engineering Physics and Thermophysics*, 76, pp. 83～92.

Naphon, P. and Wongwises, S., 2002, "An Experimental Study on the In-tube Convective Heat Transfer Coefficients in Spiral-coil Heat Exchanger," *International Communications in Heat Mass Transfer*, 29, pp. 797～809.

Naphon, P. and Wongwises, S., 2003b, "Experimental and Theoretical Investigation of the Heat Transfer Characteristics and Performance of a Spiral-coil Heat Exchanger under Dry-surface Conditions," *2nd International Conference on Heat Transfer, Fluid Mechanics, and Thermodynamics*, pp. 24-26, Victoria Falls, Zambia.

Naphon, P. and Wongwises, S., 2005a, "A Study of the Heat Transfer Characteristics of a Compact Spiral Coil Heat Exchanger under Wet-surface Conditions," *Experimental Thermal and Fluid Science*, 29, pp. 511～521.

Naphon, P. and Wongwises, S., 2005b, "Heat Transfer Coefficients under Dry-and Wet-surface Conditions for a Spirally Coiled Finned Tube Heat Exchanger," *International Communications in Heat and Mass Transfer*, 32, pp. 371～385.

Patankar, S. V. Pratap, V. S. and Spalding, D. B., 1974, "Prediction of Laminar Flow and Heat Transfer in Helically Coiled Pipes," *Journal of Fluid Mechanics*, 62, pp. 539-551.

Schmidt, T. E., 1949, "Heat Transfer Calculations for Extended Surfaces," *Refrigeration Engineering*, 49, pp. 351～357.

Xin, R. C., Awwad, A., Dong, Z. F. and Ebadian, M. A. 1997, "An Experimental Study of Single-phase and Two-phase Flow Pressure Drop in Annular Helicoidal Pipes," *International Journal of Heat and Fluid Flow*, 18, pp. 482～488.

Yang, G. and Ebadian, M. A., 1996, "Turbulent Forced Convection in a Helicoidal Pipe with Substatial Pitch," *International Journal of Heat and Mass Transfer*, 39, pp. 2015～2022.